Proceedings of the ASME 2010 3rd Joint US-European Fluids Engineering Summer Meeting and 8th International Conference on Nanochannels, Microchannels, and Minichannels
FEDSM-ICNMM2010
August 1-5, 2010, Montreal, Canada

FEDSM-ICNMM2010-30383

TURBULENCE-INDUCED VIBRATION ANALYSIS OF AN OPEN CURVED THIN SHELL

Mitra Esmailzadeh
École Polytechnique de Montreal
Mechanical Engineering Department
C.P. 6079, Succursale Centre-ville,
Montreal, Quebec, H3C 3A7,
Canada

Aouni A. Lakis
École Polytechnique de Montreal
Mechanical Engineering Department
C.P. 6079, Succursale Centre-ville,
Montreal, Quebec, H3C 3A7
Canada

ABSTRACT

A method is presented to predict the root mean square displacement response of an open curved thin shell structure subjected to a turbulent boundary-layer-induced random pressure field. The basic formulation of the dynamic problem is an efficient approach combining classic thin shell theory and the finite element method. The displacement functions are derived from Sanders' thin shell theory. A numerical approach is proposed to obtain the total root mean square displacements of the structure in terms of the cross-spectral density of random pressure fields. The cross-spectral density of pressure fluctuations in the turbulent pressure field is described using the Corcos formulation. Exact integrations over surface and frequency lead to an expression for the total root mean square displacement response in terms of the characteristics of the structure and flow. An in-house program based on the presented method was developed. The total root mean square displacements of a curved thin blade subjected to turbulent boundary layers were calculated and illustrated as a function of free stream velocity and damping ratio. A numerical implementation for the vibration of a cylinder excited by fully developed turbulent boundary layer flow was presented. The results compared favorably with those obtained using software developed by Lakis et al.

1. INTRODUCTION

Thin shells are major components in industrial structures such as skins of aircraft fuselage, hulls of ships and blades of turbines. These structures are commonly subjected to excitation forces such as turbulence, which are intrinsically random. Random pressure fluctuations induced by a turbulent boundary layer are a frequent source of excitation and can cause small amplitude vibration and eventual fatigue failure; therefore, determination of the response of shell structures to these pressures is of importance and must be below acceptable levels.

An extensive review of turbulence-induced vibration reveals that most of the studies in the literature are devoted to investigating characteristics of pressure fluctuations beneath a turbulent boundary layer. Studies on the displacement response of shell structures to these excitations are scarce. Characteristics of a turbulent boundary layer such as wall-pressure power spectral density and cross correlation functions have been extensively studied and well established [1-4].

The first theoretical study of simply supported uniform thin cylindrical shells excited by turbulent boundary layer pressure fluctuations was carried out by Cottis and Jasonides [5] based on Reissner's simplified shallow shell equations of motion. They derived a general expression for the space-time correlation function of the radial displacement of a thin cylinder with no attempt to evaluate mean square response. The first effort to make a comparison of measured and predicted simply supported thin cylindrical shell vibration when subjected to internal turbulent water flow at high frequencies was made by Clinch [6] using Powell's joint-acceptance method. Following Clinch's study, Lakis and Païdoussis [7] presented a theory using a cylindrical finite element to predict the mean square displacement of a thin cylindrical shell subjected to a pressure field arising from a turbulent boundary layer caused by internal subsonic flow.

Much research effort has been invested in evaluating the auto spectral density of the response due to a turbulent boundary layer pressure field, but no attempt to calculate total root mean square displacement response has been undertaken. For example, the auto spectral density of the velocity of a plate subjected to pressure fluctuations originating from a turbulent boundary layer was studied by Birgersson et al. [8] using spectral finite element and dynamic stiffness methods. Finnveden et al. [9] investigated the vibration response of the velocity of a thin plate excited by a turbulent boundary layer experimentally and numerically. Mazzoni [10] proposed a deterministic model based on an analytical wavenumber integration procedure to predict the power spectrum of the acceleration of a fluid-loaded thin plate subjected to turbulent flow. De Rosa and Franco[11] presented an exact and predictive response to evaluate the power spectral density of acceleration of a simply supported plate subjected to a turbulent boundary layer. Birgersson et al. [12] predicted the power spectral density of velocity of thin cylindrical shells excited by turbulent flow using Arnold-Warburton theory and the spectral finite element method; however, the effect of fluid-structure coupling was not accounted for in their analysis. Ciappi et al. [13] investigated the acceleration response spectra of a plate excited by a turbulent boundary layer pressure field experimentally and numerically. The

effect of coupled structural-fluid was taken into account in their analysis.

In the literature survey, it appears that studies on predicting the total root mean square displacement response of thin shells to random pressure fluctuations beneath a turbulent boundary layer are few. For example, an investigation was carried out by Lakis and Païdoussis [7] to determine the total root mean square displacement response of cylindrical shells to turbulent flow. Their work, however, was restricted to cylindrical forms, since a cylindrical finite element was employed. A recent work [14] was carried out by the authors in order to predict the total root mean square (rms) displacement response of a thin plate to a turbulent boundary-layer-induced random pressure field, which is only applicable to plates. However, it is clear that current models are insufficient to determine the total root mean square displacement response of open curved shell structures such as curved blades.

This study is concerned with the linear vibration of open curved thin shells, either uniform or non-uniform, due to a random pressure field arising from a turbulent boundary layer. The dynamic behavior of such structures in contact with fluid can be determined using a method previously developed by the authors [15] since dynamic characteristics of structures are needed as an input to determine the structural response due to turbulent flow. A general method is developed to predict the total root mean square displacement response of such shells to a turbulent random pressure field arising from a turbulent boundary layer. An expression for the rms displacement response of an open curved shell is obtained in terms of the wetted natural frequencies, mode shapes and other characteristics of the structure and flow. An in-house program was developed to predict the rms displacement response of an open curved thin shell structure such as a turbine blade to a random pressure field arising from a turbulent boundary layer. To validate our method, a thin cylindrical shell subjected to internally fully developed turbulent flow was studied and compared favorably with the results obtained using software developed by Lakis and Païdoussis [7].

NOMENCLATURE

A	blade length in the x-direction
B	blade width in the y-direction
C_j	unknown coefficients
$\mathbf{C}_f$	Coriolis force induced by potential flow on the structure
$\mathbf{C}_s$	global structural damping matrix of the shell structure
$\mathrm{d}A$	element surface area
d_i', d_i''	limits of the area surrounding node i in the curvilinear y-direction
$\mathbf{F}_{\mathrm{Global}}$	external load vector in global coordinates acting at each node
$\mathbf{F}_{\mathrm{Local}}$	external load vector in local coordinates acting at each node
$\mathbf{F}(f,T)$	Fourier transform of the force vector
$\mathbf{F}^*(f,T)$	complex conjugate of Fourier transforms of the force vector
$\mathbf{F}$	vector of external random forces due to turbulent boundary layer
F_n	lateral force in the local z-direction
f_r	rth natural frequency in Hz
f	excitation frequency in Hz
G_{pp}	one-sided cross-spectral density of pressure
g	gravitational acceleration
$\lvert H_r(f)\rvert$	magnification factor
$H_r(f)$	frequency response function
h	thickness of blade
h_1	height of fluid over an arbitrary element in direction normal to the element
h_2	height of fluid under an arbitrary element in direction normal to the element
i	complex number equal to $\sqrt{-1}$
$\mathbf{K}_f$	centrifugal force induced by potential flow on the structure
$\mathbf{K}_s$	global structural stiffness matrix of the shell structure
l_i, d_i	curvilinear coordinates of a typical node i in the x-and y-directions
l_i', l_i''	limits of the area surrounding node i in the curvilinear x-direction
M_x	moment in the local x-direction
M_y	moment in the local y-direction
$\mathbf{M}_f$	inertial force induced by potential flow on the structure
$[\mathbf{M}_f]_e$	fluid added virtual mass matrix of the finite element
$\mathbf{M}_s$	global structural mass matrix of the shell structure
$\bar{M}_r$	rth element of the generalized mass matrix $[\bar{\mathbf{M}}] = [\mathbf{\Phi}]^{\mathrm{T}}\left[[\mathbf{M}_s] - [\mathbf{M}_f]\right][\mathbf{\Phi}]$
m	axial wavenumber (Table 1)
$[\mathbf{N}]$	shape function matrix of the finite element
N	number of mode shapes to be used in the analysis
n	circumferential wavenumber (Table 1)
n	number of nodes
$\{\mathbf{P}\}$	fluid pressure vector applied on the shell element
$[\mathbf{P}]$	elasticity matrix
P	Fourier transform of the pressure
$P(x,y,t)$	instantaneous pressure on the surface
$\mathbf{q}(t)$	generalized coordinates vector
S_{ξ_x}	Strouhal number equal to $f\xi_x/U_C$
S_{ξ_y}	Strouhal number equal to $f\xi_y/U_C$
$[\mathbf{T}]$	nodal transformation matrix
T	period
U_C	convection velocity $U_C = 0.6U_\infty$
U_∞	free stream velocity
U_{cl}	centerline velocity
U_i	in-plane displacement of the shell reference surface in the x-direction
V_i	in-plane displacement of the shell reference surface in the y-direction
W_i	transverse displacement of the shell middle surface
$\partial W_i/\partial x$	rotation about the y-axis
$\partial W_i/\partial y$	rotation about the x-axis
x, y, z	local reference axes
$\bar{x}, \bar{y}, \bar{z}$	global reference axes (Eq. 32)

x_e	element dimension in the local x-direction (Fig. 1)
y_e	element dimension in the local y-direction (Fig. 1)
Δ	Fourier transform of the nodal displacements
δ^*	boundary layer displacement thickness
$\{\boldsymbol{\delta}_i\}$	nodal displacement at node i
$\boldsymbol{\delta}$	displacement vector of the system
$\dot{\boldsymbol{\delta}}$	velocity vector of the system
$\ddot{\boldsymbol{\delta}}$	acceleration vector of the system
$\overline{\boldsymbol{\delta}_c^2(x_c, y_c, t)}$	mean square displacement at node c
ζ_r	rth generalized damping ratio
$\theta_r(f)$	phase factor between force and response
$\Lambda_{x\bar{x}}$	cosine of the angle between local and global x-axes
ξ_x	streamwise distance of separation
ξ_y	spanwise distance of separation
ρ_f	density of the fluid
$\{\boldsymbol{\Phi}\}_r$	the rth mode shape
Φ_{ir}	irth element of the modal matrix
$\boldsymbol{\Phi}(x, y)$	modal matrix of the structure in a vacuum
$\boldsymbol{\Phi}_{cr}$	rth mode shape at node c
ϕ	velocity potential function
$\Psi(\xi_x, 0, f)$	streamwise spatial correlation function
$\Psi(0, \xi_y, f)$	spanwise spatial correlation function
$\Psi(\xi_x, \xi_y, f)$	spatial correlation function
ω	radial natural frequency
$*$	complex conjugate operator
T	matrix transpose operator
∇^2	Laplace operator

2. GOVERNING EQUATION

The dynamic behavior of a submerged shell subjected to external random loads due to a turbulent boundary layer is governed by the following equation:

$$\left[[\mathbf{M}_s]-[\mathbf{M}_f]\right]\{\ddot{\boldsymbol{\delta}}\}+\left[[\mathbf{C}_s]-[\mathbf{C}_f]\right]\{\dot{\boldsymbol{\delta}}\}+\left[[\mathbf{K}_s]-[\mathbf{K}_f]\right]\{\boldsymbol{\delta}\}=\{\mathbf{F}\} \quad (1)$$

To predict the vibration amplitude of thin structures due to turbulent boundary-layer-induced random pressure fields, one must have a comprehensive understanding of fluid-structure interaction. Dynamic characteristics of such structures in contact with stationary fluid are needed as an input to determine the root mean square displacement of the structure.

3. STRUCTURAL MODEL

In this study, the structure is modeled using a combination of classic thin shell theory and finite element analysis in which the finite elements are four-noded flat rectangular elements with five degrees of freedom per node. These degrees of freedom represent the in-plane and out-of-plane displacement components and spatial derivatives of lateral displacement (i.e. two rotations about the in-plane axes). The geometry of the shell element used in this analysis is shown in Fig. 1. The nodal displacement at node i is defined by

$$\{\boldsymbol{\delta}_i\}=\{U_i \quad V_i \quad W_i \quad \partial W_i/\partial x \quad \partial W_i/\partial y\}^{\mathrm{T}} \quad (2)$$

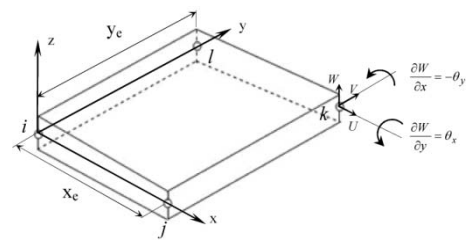

FIGURE 1. FLAT RECTANGULAR SHELL ELEMENT.

The displacement functions are derived from Sanders' thin shell equations. The flat shell element is formulated using previously available theories of membrane and plate bending elements. The solution of membrane displacements is assumed to be a bilinear polynomial and the normal displacement is determined from the shell's equation of motion instead of an arbitrary polynomial function [15]:

$$U(x,y,t)=C_1+C_2\frac{x}{A}+C_3\frac{y}{B}+C_4\frac{xy}{AB} \quad (3)$$

$$V(x,y,t)=C_5+C_6\frac{x}{A}+C_7\frac{y}{B}+C_8\frac{xy}{AB} \quad (4)$$

$$W(x,y,t)=\sum_{j=9}^{20}C_j\mathrm{e}^{\mathrm{i}\pi((x/A)+(y/B))+\mathrm{i}\omega t} \quad (5)$$

Since the out-of-plane displacement is approximated by an exponential function, which is a general solution of equilibrium equations, this method may easily be adapted to take into account hydrodynamic effects. Moreover, this method is capable of calculating both high and low frequencies with high accuracy. Although this capability is normally of little interest in free vibration analysis, it is of considerable importance for determining the response of curved structures subjected to random pressure fields such as those generated by turbulent flow.

The displacement functions can be written in matrix form as follows:

$$\{U \quad V \quad W\}^{\mathrm{T}}=[\mathbf{R}][\mathbf{A}]^{-1}\{\boldsymbol{\delta}\}_{\mathrm{e}}=[\mathbf{N}]\{\boldsymbol{\delta}\}_{\mathrm{e}} \quad (6)$$

where matrices $[\mathbf{R}]$ and $[\mathbf{A}]^{-1}$ are given in Ref. [15] and $\{\boldsymbol{\delta}\}_{\mathrm{e}}$ is the nodal displacement of the element given as:

$$\{\boldsymbol{\delta}\}_{\mathrm{e}}=\left\{\{\boldsymbol{\delta}_i\}^{\mathrm{T}},\{\boldsymbol{\delta}_j\}^{\mathrm{T}},\{\boldsymbol{\delta}_k\}^{\mathrm{T}},\{\boldsymbol{\delta}_l\}^{\mathrm{T}}\right\}^{\mathrm{T}} \quad (7)$$

The strain-displacement relationship is given by

$$\{\boldsymbol{\varepsilon}\}=\left\{\frac{\partial U}{\partial x} \quad \frac{\partial V}{\partial y} \quad \frac{\partial U}{\partial y}+\frac{\partial V}{\partial x} \quad \frac{-\partial^2 W}{\partial x^2} \quad \frac{-\partial^2 W}{\partial y^2} \quad \frac{-2\partial^2 W}{\partial x\partial y}\right\}^{\mathrm{T}} \quad (8)$$

Substituting the displacements, the strain vector is obtained in terms of the nodal displacements as follows:

$$\{\boldsymbol{\varepsilon}\}=[\mathbf{Q}][\mathbf{A}]^{-1}\{\boldsymbol{\delta}\}_{\mathrm{e}}=[\mathbf{B}]\{\boldsymbol{\delta}\}_{\mathrm{e}} \quad (9)$$

where matrix $[\mathbf{Q}]$ is a 6×20 matrix given in Ref. [15].

The rigidity and mass matrices of a single rectangular finite element in its local coordinates are given by finite element theory:

$$[\mathbf{K}]_{\mathrm{e}}=\iint_A[\mathbf{B}]^{\mathrm{T}}[\mathbf{P}][\mathbf{B}]\mathrm{d}A \quad (10)$$

$$[\mathbf{M}]_{\mathrm{e}}=\rho_s h\iint_A[\mathbf{N}]^{\mathrm{T}}[\mathbf{N}]\mathrm{d}A \quad (11)$$

Substituting matrices $[\mathbf{B}]$ and $[\mathbf{N}]$, the structural mass and stiffness matrices can be determined analytically by exact integrations over x and y as follows:

$$[\mathbf{K}]_{\mathrm{e}} = [\mathbf{A}]^{-\mathrm{T}} \left(\int_0^{y_{\mathrm{e}}} \int_0^{x_{\mathrm{e}}} [\mathbf{Q}]^{\mathrm{T}} [\mathbf{P}][\mathbf{Q}] \mathrm{d}x\mathrm{d}y \right) [\mathbf{A}]^{-1} \tag{12}$$

$$[\mathbf{M}]_{\mathrm{e}} = [\mathbf{A}]^{-\mathrm{T}} \left(\rho_s h \int_0^{y_{\mathrm{e}}} \int_0^{x_{\mathrm{e}}} [\mathbf{R}]^{\mathrm{T}} [\mathbf{R}] \mathrm{d}x\mathrm{d}y \right) [\mathbf{A}]^{-1} \tag{13}$$

The global structural mass and stiffness matrices can be computed using the transformation matrix given in Eq. (32) and assembling techniques.

4. FLUID MODEL

The inviscid incompressible flow is modeled using linear potential flow. The velocity potential function ϕ satisfies the Laplace equation throughout the fluid domain:

$$\nabla^2 \phi = \frac{\partial^2 \phi}{\partial x^2} + \frac{\partial^2 \phi}{\partial y^2} + \frac{\partial^2 \phi}{\partial z^2} = 0 \tag{14}$$

The dynamic condition at the interface of a stationary fluid and shell can be determined using the Bernoulli's equation as follows:

$$P\Big|_{\text{at the wall}} = -\rho_f \frac{\partial \phi}{\partial t} \tag{15}$$

The impermeability condition ensures permanent contact at the interface of the fluid and shell, stating that the fluid normal velocity at the interface matches the instantaneous rate of change of the normal displacement of the shell:

$$\frac{\partial \phi}{\partial z}\Big|_{\text{at the wall}} = \frac{\partial W}{\partial t} \tag{16}$$

A free surface and rigid wall are considered as fluid boundary conditions for a submerged blade, respectively, as follows:

$$\frac{\partial \phi}{\partial z}\Big|_{z=h_1} = -\frac{1}{g}\frac{\partial^2 \phi}{\partial t^2} \quad , \quad \frac{\partial \phi}{\partial z}\Big|_{z=-h-h_2} = 0 \tag{17}$$

Putting all of these together, the fluid pressure applied on each element is determined by combining the velocity potential function, Bernoulli's equation, the impermeability condition and the boundary conditions of the fluid and is expressed as a function of acceleration of the normal displacement of the structure and the inertial force of the quiescent fluid as follows [15]:

$$P = -\rho_f \left(\frac{1 - \mathrm{e}^{2\mu h_1}}{\mu(1 + \mathrm{e}^{2\mu h_1})} - \frac{1 + \mathrm{e}^{2\mu h_2}}{\mu(\mathrm{e}^{2\mu h_2} - 1)} \right) \frac{\partial^2 W}{\partial t^2} = -\rho_f Z_f \frac{\partial^2 W}{\partial t^2} \tag{18}$$

where the coefficient Z_f depends on the fluid-structure contact model and μ is defined as $\mu = \pi \sqrt{\frac{1}{A^2} + \frac{1}{B^2}}$.

The fluid-induced force vector can be obtained by an analytical integration of the product of the structural shape function and fluid pressure over the fluid-structure interface area of the element. The inertial force of a stationary fluid is obtained, which is interpreted as the added virtual mass matrix of the fluid:

$$\{\mathbf{F}\}_{\mathrm{e}} = \rho_f Z_f [\mathbf{A}]^{-\mathrm{T}} \left(\int_0^{y_{\mathrm{e}}} \int_0^{x_{\mathrm{e}}} [\mathbf{R}]^{\mathrm{T}} [\mathbf{R}_f] \mathrm{d}x\,\mathrm{d}y \right) [\mathbf{A}]^{-1} \{\ddot{\boldsymbol{\delta}}\}_{\mathrm{e}} = [\mathbf{M}_f]_{\mathrm{e}} \{\ddot{\boldsymbol{\delta}}\}_{\mathrm{e}} \tag{19}$$

where matrices $[\mathbf{R}]$, $[\mathbf{A}]^{-1}$ and $[\mathbf{R}_f]$ are given in Ref. [15]. The global fluid mass matrix can be computed using the transformation matrix given in Eq. (32) and assembling techniques.

5. FLUID-STRUCTURE MODEL

The dynamic behavior of a structure is affected by the presence of fluid. The fluid pressure applied on a structure can be expressed as a function of displacement, velocity and acceleration. These forces are interpreted as centrifugal, Coriolis and inertial effects of the fluid, respectively. The fluid force matrices are superimposed onto the structural matrices to form the dynamic equations of a coupled fluid-structure system.

The dynamic behavior of a shell subjected to a potential flow can be represented as follows:

$$\left[[\mathbf{M}_s] - [\mathbf{M}_f]\right]\{\ddot{\boldsymbol{\delta}}\} + \left[[\mathbf{C}_s] - [\mathbf{C}_f]\right]\{\dot{\boldsymbol{\delta}}\} + \left[[\mathbf{K}_s] - [\mathbf{K}_f]\right]\{\boldsymbol{\delta}\} = \{\mathbf{0}\} \tag{20}$$

The magnitude of the centrifugal and Coriolis forces changes directly with flow velocity and fluid density, and inversely with Young's modulus of the structure. Therefore, when we are dealing with metal shells in the vicinity of fluid with flow velocity in the normal engineering range, the effects of fluid damping and stiffness are small and can be neglected without significant loss of accuracy on the dynamic behavior of the structure. The effects of the flow on the shell can therefore be considered the same as the effects of a stationary fluid in contact with the shell. The global equations of motion of a shell subjected to potential flow can be reduced to the following system:

$$\left[[\mathbf{M}_s] - [\mathbf{M}_f]\right]\{\ddot{\boldsymbol{\delta}}\} + [\mathbf{C}_s]\{\dot{\boldsymbol{\delta}}\} + [\mathbf{K}_s]\{\boldsymbol{\delta}\} = \{\mathbf{0}\} \tag{21}$$

6. TURBULENCE MODEL

The pressure field arising from a fully developed turbulent boundary layer in subsonic flow is intrinsically random; therefore, the statistical properties of the turbulent flow must be employed. Statistical properties of wall-pressure fluctuations of turbulent boundary layers are utilized to obtain vibration amplitude. We assume the random process is stationary ergodic and the random pressure fluctuation is homogeneous. Therefore mean square displacement response can be expressed in terms of the cross spectral density (CSD) of the pressure field. The wall-pressure CSD is approximated by semi-empirical models.

The Corcos model for the CSD of the pressure fluctuations is adopted to describe the turbulent pressure field. In the Corcos model the CSD of the pressure is formulated as the product of the power spectral density (PSD) of the pressure and the wall-pressure cross correlation function as follows:

$$G_{pp}(\xi_x, \xi_y, f) = G_{pp}(f)\Psi(\xi_x, \xi_y, f) \tag{22}$$

Corcos suggested that a correlation function between two points in an oblique direction can be presented by the product of the lateral and longitudinal correlation functions [16]:

$$\Psi(\xi_x, \xi_y, f) = \Psi(\xi_x, 0, f)\Psi(0, \xi_y, f) \tag{23}$$

Corcos postulated that the longitudinal and lateral correlations may be expressed as an exponentially decaying oscillating function in the flow direction and a simple exponentially decaying function in the cross-flow direction respectively, as follows:

$$\Psi(\xi_x, 0, f) = \mathrm{e}^{-\alpha_x 2\pi \left|S_{\xi_x}\right|} \mathrm{e}^{\mathrm{i}2\pi S_{\xi_x}} \ , \ \Psi(0, \xi_y, f) = \mathrm{e}^{-\alpha_y 2\pi \left|S_{\xi_y}\right|} \tag{24}$$

where α_x and α_y are empirically determined constants. Blake recommends that α_x = 0.116 and α_y = 0.7 be used for smooth walls [17].

The power spectral density of wall pressure beneath a turbulent boundary layer is the most significant characteristic of turbulent flow, which is similar in terms of both feature and magnitude for different

structures subjected to various fluids. For example, the power spectral density of the turbulent wall pressure fluctuations on a body of revolution in a water medium was obtained by Bakewell [18] and the result was in good agreement with pressure data obtained on flat plates and in fully developed turbulent pipe flow. The general trends of wall-pressure power spectral density obtained by Bakewell et al. in pipe airflow, by Clinch in pipe water flow, by Willmarth and Wooldridge over a flat plate boundary layer, and in a straight flow channel are similar as shown by Au-Yang [19]. Therefore, it seems that the one-sided power spectral density of wall pressure proposed by Lakis and Païdoussis [7] based on Bakewell's measurements in pipe airflow [1] is applicable to an open curved thin shell such as a blade as follows [7]:

$$G_{pp}(f) = k_2\, \rho_f^2\, \delta^* U_\infty^3\, \mathrm{e}^{-k_1 \delta^* f / U_\infty} \tag{25}$$

where $k_1 = 0.25$, $k_2 = 2\times10^{-6}$.

7. RESPONSE TO TURBULENT FLOW

7.1. Decoupling of the equations of motion

The shell response $\boldsymbol{\delta}(x,y,t)$ at any point *x, y* and at any time *t* may be expressed as a normal mode expansion in terms of the generalized coordinates vector $\mathbf{q}(t)$ and the modal matrix in a vacuum $\boldsymbol{\Phi}(x,y)$ as follows:

$$\{\boldsymbol{\delta}(x,y,t)\} = [\boldsymbol{\Phi}(x,y)]\{\mathbf{q}(t)\} \tag{26}$$

Substituting the above relationship into Eq. (1), pre-multiplying by $\boldsymbol{\Phi}^{\mathrm{T}}$ and then adopting the viscous damping type of structural damping into the equation of motion, the uncoupled set of equations is obtained as follows:

$$\ddot{q}_r + 4\pi\zeta_r f_r \dot{q}_r + 4\pi^2 f_r^2 q_r = \frac{1}{\bar{M}_r}\{\boldsymbol{\Phi}\}_r^{\mathrm{T}}\{\mathbf{F}\} \qquad r = 1,2,\ldots,N \tag{27}$$

Upon solving the above equation the instantaneous response at a typical node *c*, $\boldsymbol{\delta}_c$ in terms of the generalized coordinates is found:

$$\{\boldsymbol{\delta}_c(x,y,t)\} = \sum_{r=1}^{N}\{\boldsymbol{\Phi}_{cr}(x_c,y_c)\}\, q_r(t) \tag{28}$$

7.2. Representation of a continuous random pressure field at the nodal points

The continuous random pressure field acting on the shell will be approximated by a finite set of discrete forces and moments acting at the nodal points. The shell is divided into finite elements, each of which is a rectangular flat shell element. A pressure field is considered to be acting on an area S_c surrounding the node *c* of the coordinates l_c and d_c as shown in Fig. 2. This area S_c is delimited by the positions l_c' and l_c'' with respect to the origin in the curvilinear *x*-direction and d_c' and d_c'' with respect to the origin in the curvilinear *y*-direction. The lateral force acting at an arbitrary point *A* on the area S_c is given by:

$$F_A(t) = \int_{d_c'}^{d_c''}\int_{l_c'}^{l_c''} P(x,y,t)\,\mathrm{d}x\,\mathrm{d}y \tag{29}$$

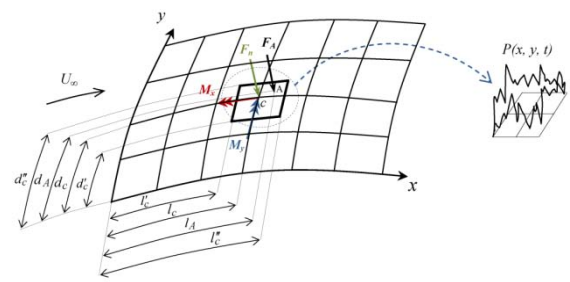

FIGURE 2. TRANSFORMATION OF A CONTINUOUS PRESSURE FIELD INTO A DISCRETE FORCE FIELD ACTING AT NODE *C*.

This force is transformed into one force and two moments acting at node *c*, as illustrated in Fig. 2. The external load vector in local coordinates acting at a typical point *c* can be written in the following form:

$$\{\mathbf{F}(t)\}_{\text{Local}} = \begin{Bmatrix} 0 \\ 0 \\ F_n \\ M_y \\ M_x \\ 0 \end{Bmatrix}_{\text{Local}} = \begin{Bmatrix} 0 \\ 0 \\ -\int_{d_i'}^{d_i''}\int_{l_i'}^{l_i''} P(x_i,y_i,t)\,\mathrm{d}x_i\,\mathrm{d}y_i \\ -\int_{d_i'}^{d_i''}\int_{l_i'}^{l_i''} (x_i - l_i)P(x_i,y_i,t)\,\mathrm{d}x_i\,\mathrm{d}y_i \\ -\int_{d_i'}^{d_i''}\int_{l_i'}^{l_i''} (y_i - d_i)P(x_i,y_i,t)\,\mathrm{d}x_i\,\mathrm{d}y_i \\ 0 \end{Bmatrix} \tag{30}$$

The external load vector in global coordinates acting at each node is obtained using the relation:

$$\{\mathbf{F}\}_{\text{Global}} = [\mathbf{T}]\{\mathbf{F}\}_{\text{Local}} \tag{31}$$

The nodal transformation matrix made up of the direction cosines expressed as follows (see Ref. [20] for more details):

$$[\mathbf{T}] = \begin{bmatrix} \Lambda_{x\bar{x}} & \Lambda_{y\bar{x}} & \Lambda_{z\bar{x}} & 0 & 0 & 0 \\ \Lambda_{x\bar{y}} & \Lambda_{y\bar{y}} & \Lambda_{z\bar{y}} & 0 & 0 & 0 \\ \Lambda_{x\bar{z}} & \Lambda_{y\bar{z}} & \Lambda_{z\bar{z}} & 0 & 0 & 0 \\ 0 & 0 & 0 & \Lambda_{y\bar{y}} & -\Lambda_{x\bar{y}} & -\Lambda_{z\bar{y}} \\ 0 & 0 & 0 & -\Lambda_{y\bar{x}} & \Lambda_{x\bar{x}} & \Lambda_{z\bar{x}} \\ 0 & 0 & 0 & -\Lambda_{y\bar{z}} & \Lambda_{x\bar{z}} & \Lambda_{z\bar{z}} \end{bmatrix} \tag{32}$$

7.3. Mean square response of a thin structure to an arbitrary homogenous random pressure

A random process can only be described in statistical terms. Here, we assume that the random pressure is stationary in time and homogeneous in space so the response can be expressed in terms of the cross spectral density of the pressure. Assuming that we are dealing with an ergodic process and using the correlation theorem, the mean square displacement response at node *c* can be expressed as follows:

$$\overline{\boldsymbol{\delta}_c^2(x_c,y_c,t)} = \lim_{T\to\infty}\frac{1}{T}\int_0^{+\infty} \boldsymbol{\Delta}_c^*(x_c,y_c,f,T).\boldsymbol{\Delta}_c(x_c,y_c,f,T)\,\mathrm{d}f \tag{33}$$

Taking the Fourier transform of Eq. (27) and then introducing the Fourier transform of the generalized coordinates into the Fourier transform of Eq. (28), the Fourier transform of the nodal displacement can be written as follows:

$$\mathbf{\Delta}_c(f,T)=\sum_{r=1}^{N}\mathbf{\Phi}_{cr}\frac{|H_r(f)|\mathrm{e}^{-\mathrm{i}\theta_r(f)}}{4\pi^2 f_r^2\bar{M}_r}\mathbf{\Phi}_r^{\mathrm{T}}\mathbf{F}(f,T) \tag{34}$$

The frequency response function for the rth mode defined as follows:

$$H_r(f)=\left\{1-\left(\frac{f}{f_r}\right)^2+2\mathrm{i}\zeta_r\left(\frac{f}{f_r}\right)\right\}^{-1}=|H_r(f)|\mathrm{e}^{-\mathrm{i}\theta_r(f)} \tag{35}$$

Introducing Eq. (34) and its complex conjugate into Eq. (33), the mean square response at node c is obtained:

$$\overline{\delta_c^2(x_c,y_c,t)}=\sum_{r=1}^{N}\sum_{s=1}^{N}\frac{\mathbf{\Phi}_{cr}(x_c,y_c)\mathbf{\Phi}_{cs}(x_c,y_c)}{(2\pi)^4 f_r^2 f_s^2\bar{M}_r\bar{M}_s}\lim_{T\to\infty}\frac{1}{T}\int_0^{\infty}\mathrm{e}^{\mathrm{i}(\theta_s-\theta_r)}|H_r(f)||H_s(f)| \times\{\mathbf{\Phi}\}_s^{\mathrm{T}}\mathbf{F}^*(f,T)\{\mathbf{\Phi}\}_r^{\mathrm{T}}\mathbf{F}(f,T)\mathrm{d}f \tag{36}$$

For a lightly damped multi-degree-of-freedom system with well-separated natural frequencies, the cross-product terms are small in comparison to the self-product terms. Therefore, the contribution of the cross-product terms to the mean square displacement response can be ignored without significant loss of accuracy. Eq. (36) can now be rewritten as follows:

$$\overline{\delta_c^2(x_c,y_c,t)}=\sum_{r=1}^{N}\frac{\mathbf{\Phi}_{cr}^2(x_c,y_c)}{16\pi^4 f_r^4\bar{M}_r^2}\lim_{T\to\infty}\frac{1}{T}\int_0^{\infty}|H_r(f)|^2\{\mathbf{\Phi}\}_r^{\mathrm{T}}\mathbf{F}(f,T)\{\mathbf{\Phi}\}_r^{\mathrm{T}}\mathbf{F}^*(f,T)\mathrm{d}f \tag{37}$$

Substituting the Fourier transform of the external force vector from Eq. (31) and its complex conjugate into Eq. (37) and transforming the vector by summation, the mean square response is obtained in terms of the one-sided cross-spectral density of pressure.

The one-sided cross-spectral density of pressure is defined as follows:

$$G_{pp}(x_i,y_i,x_j,y_j,f)=\lim_{T\to\infty}\frac{1}{T}P^*(x_i,y_i,f,T)P(x_j,y_j,f,T) \tag{38}$$

The cross-spectral density of a homogenous pressure field can be expressed in terms of distances of separation (ξ_x and ξ_y) along the curvilinear coordinates instead of the coordinates themselves. Therefore, the one-sided cross-spectral density of pressure can be written as

$$G_{pp}(\xi_x,\xi_y,f)=\lim_{T\to\infty}\frac{1}{T}P(x_i,y_i,f,T)P^*(x_u,y_u,f,T) \tag{39}$$

7.4. Mean square response due to a turbulent boundary layer pressure field

The expressions of the wall-pressure PSD, longitudinal and lateral correlations are introduced into the mean square displacement expression. Exact integrations over surface and frequency are carried out analytically and an expression for the mean square displacement response is obtained in terms of the wetted natural frequencies, undamped mode shapes, generalized mass of the system and other characteristics of the structure and flow as follows:

$$\overline{\delta_c^2(x_c,y_c,t)}=\sum_{r=1}^{N}\frac{\mathbf{\Phi}_{cr}^2}{16\pi^4 f_r^4\bar{M}_r^2}\left(\sum_{b=1}^{6}R_b(\Phi_{ir},f_r,\zeta_r,U_C,U_\infty,\rho_f,\delta^*,l_i,l_i',l_i'',d_i,d_i',d_i'')\right) \tag{40}$$

where R_b's are complicated expressions. Here, only R_1 is given:

$$\begin{aligned}R_1=&\sum_{m=1}^{n}\sum_{q=1}^{n}\Phi_{mr}\Phi_{qr}\Lambda_{\bar{z}_m}x_m\Lambda_{\bar{z}_q}x_q\left|(\Gamma_{F_nF_n})_{mq}\right|+\sum_{m=1}^{n}\sum_{o=1}^{n}\Phi_{mr}\Phi_{or}\Lambda_{\bar{z}_m}x_m\Lambda_{\bar{z}_o}y_o\left|(\Gamma_{F_nF_n})_{mo}\right|\\&+\sum_{m=1}^{n}\sum_{u=1}^{n}\Phi_{mr}\Phi_{ur}\Lambda_{\bar{z}_m}x_m\Lambda_{\bar{z}_u}z_u\left|(\Gamma_{F_nF_n})_{mu}\right|+\sum_{m=1}^{n}\sum_{k=1}^{n}\Phi_{mr}\Phi_{kr}\Lambda_{\bar{z}_m}x_m\Lambda_{\bar{y}_k}y_k\left|(\Gamma_{F_nM_y})_{mk}\right|\\&-\sum_{m=1}^{n}\sum_{k=1}^{n}\Phi_{mr}\Phi_{kr}\Lambda_{\bar{z}_m}x_m\Lambda_{\bar{x}_k}y_k\left|(\Gamma_{F_nM_x})_{mk}\right|-\sum_{m=1}^{n}\sum_{v=1}^{n}\Phi_{mr}\Phi_{vr}\Lambda_{\bar{z}_m}x_m\Lambda_{\bar{y}_v}x_v\left|(\Gamma_{F_nM_y})_{mv}\right|\\&+\sum_{m=1}^{n}\sum_{v=1}^{n}\Phi_{mr}\Phi_{vr}\Lambda_{\bar{z}_m}x_m\Lambda_{\bar{x}_v}x_v\left|(\Gamma_{F_nM_x})_{mv}\right|-\sum_{m=1}^{n}\sum_{h=1}^{n}\Phi_{mr}\Phi_{hr}\Lambda_{\bar{z}_m}x_m\Lambda_{\bar{y}_h}z_h\left|(\Gamma_{F_nM_y})_{mh}\right|\\&+\sum_{m=1}^{n}\sum_{h=1}^{n}\Phi_{mr}\Phi_{hr}\Lambda_{\bar{z}_m}x_m\Lambda_{\bar{x}_h}z_h\left|(\Gamma_{F_nM_x})_{mh}\right|\end{aligned} \tag{41}$$

where $\Gamma_{F_nF_n}$, $\Gamma_{F_nM_x}$, $\Gamma_{F_nM_y}$, $\Gamma_{M_xM_x}$, $\Gamma_{M_yM_y}$ and $\Gamma_{M_xM_y}$ are complicated functions, too long to give here. Only $\Gamma_{F_nF_n}$ is given in detail. Note that the indices m and q are associated with forces in the x-direction, o with force in the y-direction, u with lateral force in the z-direction, k with moment about x, v with moment about y, and h with moment about z.

$$(\Gamma_{F_nF_n})_{mq}=\frac{K_2}{C^2(A^2+B^2)^2}\times\begin{Bmatrix}(B^2-A^2)\left[F_4^c(l_m',l_q',d_m',d_q')+F_4^c(l_m'',l_q'',d_m',d_q')-F_4^c(l_m',l_q'',d_m',d_q')-F_4^c(l_m'',l_q',d_m',d_q')\right]\\-(2AB)\left[F_4^s(l_m',l_q',d_m',d_q')+F_4^s(l_m'',l_q'',d_m',d_q')-F_4^s(l_m',l_q'',d_m',d_q')-F_4^s(l_m'',l_q',d_m',d_q')\right]\\+(B^2-A^2)\left[F_4^c(l_m',l_q',d_m'',d_q'')+F_4^c(l_m'',l_q'',d_m'',d_q'')-F_4^c(l_m',l_q'',d_m'',d_q'')-F_4^c(l_m'',l_q',d_m'',d_q'')\right]\\-(2AB)\left[F_4^s(l_m',l_q',d_m'',d_q'')+F_4^s(l_m'',l_q'',d_m'',d_q'')-F_4^s(l_m',l_q'',d_m'',d_q'')-F_4^s(l_m'',l_q',d_m'',d_q'')\right]\\-(B^2-A^2)\left[F_4^c(l_m',l_q',d_m'',d_q')+F_4^c(l_m'',l_q'',d_m'',d_q')-F_4^c(l_m',l_q'',d_m'',d_q')-F_4^c(l_m'',l_q',d_m'',d_q')\right]\\+(2AB)\left[F_4^s(l_m',l_q',d_m'',d_q')+F_4^s(l_m'',l_q'',d_m'',d_q')-F_4^s(l_m',l_q'',d_m'',d_q')-F_4^s(l_m'',l_q',d_m'',d_q')\right]\\-(B^2-A^2)\left[F_4^c(l_m',l_q',d_m',d_q'')+F_4^c(l_m'',l_q'',d_m',d_q'')-F_4^c(l_m',l_q'',d_m',d_q'')-F_4^c(l_m'',l_q',d_m',d_q'')\right]\\+(2AB)\left[F_4^s(l_m',l_q',d_m',d_q'')+F_4^s(l_m'',l_q'',d_m',d_q'')-F_4^s(l_m',l_q'',d_m',d_q'')-F_4^s(l_m'',l_q',d_m',d_q'')\right]\end{Bmatrix} \tag{42}$$

where

$$\begin{aligned}F_4^c(l_i',l_u',d_i',d_u')&=\int_0^{\infty}\frac{\mathrm{e}^{-\left[K_1+C|d_i'-d_u'|+B|l_i'-l_u'|\right]f}\cos(A|l_i'-l_u'|f)}{f^4\left[\frac{f^4}{f_r^4}+(\frac{4\zeta_r^2-2}{f_r^2})f^2+1\right]}\mathrm{d}f\\&=\frac{\pi}{8f_r^3}\left(5\mathrm{e}^{-\gamma_1}\sin\gamma_2-5\mathrm{e}^{-\gamma_3}\sin\gamma_4+\frac{1}{\zeta_r}\left(\mathrm{e}^{-\gamma_1}\cos\gamma_2+\mathrm{e}^{-\gamma_3}\cos\gamma_4\right)\right)\end{aligned} \tag{43}$$

$$\begin{aligned}F_4^s(l_i',l_u',d_i',d_u')&=\int_0^{\infty}\frac{\mathrm{e}^{-\left[K_1+C|d_i'-d_u'|+B|l_i'-l_u'|\right]f}\sin(A|l_i'-l_u'|f)}{f^4\left[\frac{f^4}{f_r^4}+(\frac{4\zeta_r^2-2}{f_r^2})f^2+1\right]}\mathrm{d}f\\&=\frac{\pi}{8f_r^3}\left(-5\mathrm{e}^{-\gamma_1}\cos\gamma_2+5\mathrm{e}^{-\gamma_3}\cos\gamma_4+\frac{1}{\zeta_r}\left(\mathrm{e}^{-\gamma_1}\sin\gamma_2+\mathrm{e}^{-\gamma_3}\sin\gamma_4\right)\right)\end{aligned} \tag{44}$$

and

$$\gamma_1(l_i',l_u',d_i',d_u')=\left[K_1+C|d_i'-d_u'|+(A\zeta_r+B)|l_i'-l_u'|\right]f_r \tag{45}$$

$$\gamma_2(l_i',l_u',d_i',d_u')=\left[-K_1\zeta_r-C\zeta_r|d_i'-d_u'|+(A-B\zeta_r)|l_i'-l_u'|\right]f_r \tag{46}$$

$$\gamma_3(l_i',l_u',d_i',d_u')=\left[K_1+C|d_i'-d_u'|-(A\zeta_r-B)|l_i'-l_u'|\right]f_r \tag{47}$$

$$\gamma_4(l_i', l_u', d_i', d_u') = \left[K_1 \zeta_r + C\zeta_r \left| d_i' - d_u' \right| + (A + B\zeta_r) \left| l_i' - l_u' \right| \right] f_r \quad (48)$$

where the constants are given as follows:

$$A = \frac{2\pi}{U_C},\ B = \frac{\alpha_x 2\pi}{U_C},\ C = \frac{\alpha_y 2\pi}{U_C},\ K_1 = \frac{k_1 \delta^*}{U_\infty},\ K_2 = k_2 \rho_f^2 \delta^* U_\infty^3$$

These sophisticated expressions are implemented in an in-house program to predict the total root mean square displacement response of curved thin structures. The input damping ratio and parameters related to the flow field are assumed to be known from experimental data while the added virtual mass and wetted natural frequency effects due to hydrodynamic loading of the structure are included in the analysis.

8. NUMERICAL RESULTS

8.1. Verification of the method

In order to validate our method, a thin cylindrical shell clamped at both ends whose length, radius and thickness are 0.664 m, 0.175 m and 0.001 m, respectively was studied. The material properties are; Young's modulus $E = 2.06\times10^{11}$ Pa, Poisson's ratio ν = 0.3 and density ρ_s = 7680 kg m^{-3}. The damping ratio of the shell is ζ = 0.01 for all modes. Water is flowing through the cylinder with a centerline velocity (U_{cl}) of 25 m s^{-1}. The cylinder is discretized into 32 and 22 flat shell elements in circumferential and longitudinal directions, respectively.

To validate the calculation, the maximum total rms response of the shell was obtained using the software developed by Lakis and Païdoussis [7], in which the cylindrical frustum was used as a finite element. The cylindrical finite element was bounded at its extremity by two circular nodes, with four degrees of freedom per node that represent three translations in axial, circumferential and radial directions, and one spatial derivative of normal displacement with respect to the axial direction. This software is a reliable computer code which has been employed for more than three decades to study dynamic behavior of thin cylindrical shells in a vacuum [21], in quiescent fluid [22, 23], in flowing fluid [24] and subjected to turbulent boundary-layer-induced random pressure fields [7]. The cylindrical shell was subdivided into 10 identical cylindrical finite elements. The first few natural frequencies of the fluid-filled clamped cylinder were calculated using the present method and compared with those obtained using the software developed by Lakis et al. in Table 1. Good agreement between the present method and Lakis' theory was found.

TABLE 1. COMPARISON OF THE NATURAL FREQUENCIES OF A FLUID-FILLED CYLINDER.

	Coupled natural frequency (Hz)		Discrepancy (%)
(n,m)	Lakis' method (cylindrical finite element)	Present method (flat shell element)	
(5,1)	138.44	139.49	0.75
(4,1)	152.61	147.90	3.18
(6,1)	158.24	167.83	5.70
(3,1)	201.73	180.24	11.92
(7,1)	205.59	227.21	9.52

The maximum total rms radial displacement at the axial-midpoint of the aforementioned thin cylindrical shell subjected to internally fully developed turbulent flow was obtained using the present method and compared with that obtained using the method developed by Lakis as listed in Table 2. The total mean square response was obtained by summation of mean square response over significant modes of the system. The calculation of the total response using Lakis' method was confined to the circumferential modes from n=2 to 9 and for the first 10 corresponding axial modes. In our method, the total response was obtained by summation of the mean square response for the first 22 natural frequencies from 139.49 to 425.32 Hz. In our proposed method, the Corcos lateral and longitudinal correlations were used, but in Lakis' results, Bakewell correlations were employed. Even though different correlations were adapted in the numerical calculations, good agreement was achieved.

TABLE 2. COMPARISON OF THE MAXIMUM TOTAL RMS RADIAL DISPLACEMENT OF A THIN CYLINDRICAL SHELL SUBJECTED TO INTERNALLY FULLY DEVELOPED TURBULENT BOUNDARY LAYER FOR U_{cl} =25 m s^{-1} AND ζ=10^{-2}.

Max. total rms radial displacement (m)		Discrepancy (%)
Lakis' method	Present method	
2.12533E-05	2.05761E-05	3.29

8.2 Response of a thin blade subjected to turbulent boundary-layer-induced random pressure fields

Consider a curved thin blade, which is clamped at one short side as shown in Fig. 3. The blade has a length of 0.15 m, a width of 0.1 m and a thickness of 0.005 m. The material properties are: Young's modulus $E = 2\times10^{11}$ Pa, Poisson's ratio ν = 0.3 and density ρ_s = 7970 kg m^{-3}. The boundary layer displacement thickness is assumed equal to 0.00018 m in the calculation of the response. The blade is discretized into 30×40 flat rectangular elements. The natural frequencies of the blade in a vacuum were calculated and compared favorably with those obtained using ANSYS as listed in Table 3.

TABLE 3. COMPARISON OF THE NATURAL FREQUENCIES OF A CLAMPED BLADE IN A VACUUM.

Natural frequency (Hz)		Discrepancy (%)
ANSYS (SHELL63)	Present method (Flat rectangular element)	
185.10	186.08	0.52
646.31	648.07	0.27
1142.90	1144.63	0.15
2135.80	2136.32	0.02
2772.90	2770.90	0.07
2925.30	2929.33	0.14

Natural frequencies of the abovementioned blade completely submerged in quiescent water far from fluid extremities were calculated using our method. The first mode shapes of the curved blade in a vacuum at 186.08 Hz and submerged in still water far from fluid extremities at 122.10 Hz were visualized using TECPLOT and compared with the undeformed blade as shown in Fig. 3.

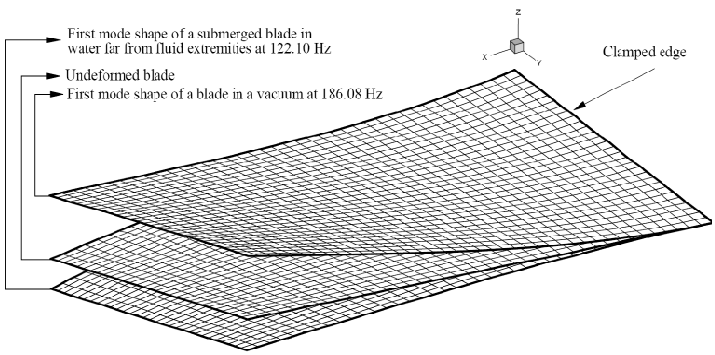

FIGURE 3. FIRST MODE SHAPES OF A BLADE IN A VACUUM AND SUBMERGED IN STILL WATER AS COMPARED TO AN UNDEFORMED BLADE.

It is worth mentioning that the level of fluid over and under the blade as well as the boundary conditions of the fluid (namely free surface, rigid wall or elastic object) affect the dynamic behavior of the blade until a certain height of fluid is reached (50 percent of the length of the blade) [15]. Table 4 shows the convergence of the natural frequencies of the system. It is observed that convergence has been reached for a mesh of 30×40 and refining the mesh beyond that does not affect the natural frequencies of the system.

TABLE 4. CONVERGENCE OF THE COUPLED NATURAL FREQUENCIES OF A BLADE BOUNDED BY FAR-OFF FLUID EXTREMITIES.

Coupled natural frequency (Hz)			
Mesh 10×20	Mesh 20×30	Mesh 30×40	Mesh 35×45
123.26	122.27	122.10	122.08
425.94	424.95	424.64	424.57
754.33	752.70	752.40	752.35
1400.07	1399.82	1399.74	1399.72
1881.42	1880.33	1880.04	1879.97
2167.32	2163.40	2162.60	2162.43

Based on the preceding analysis, the total rms displacement responses of the blade were obtained by summation over all significant modes of vibration at all nodes and then the maximum total rms response of the blade was calculated. It can be clearly seen from Eq. (40) that the rms response is inversely proportional to the square of the natural frequency. This therefore indicates that the first four natural frequencies suffice to calculate the total response for the blade studied here. The effect of mesh refinement on the maximum total rms displacements of the blade subjected to a turbulent boundary layer from both sides where fluid is flowing along the short side of the blade for $U_\infty = 16$ m s^{-1} and $\zeta = 10^{-3}$ is presented in Table 5.

It is observed that mesh refinement beyond 30×40 has almost no considerable effect on the response and the total rms displacements differ by about 8 percent. Therefore, a mesh of 30×40 is used for further calculations. The maximum total rms displacements versus free stream velocity in the range of 4-24 m s^{-1} and for damping ratios 10^{-2} and 10^{-3} for the clamped blade subjected to turbulent boundary layer from both sides, where water is flowing along the short side of the blade are depicted in Fig. 4. The geometry of the undeformed blade is also shown in Fig. 4.

TABLE 5. COMPARISON OF THE MAXIMUM TOTAL RMS DISPLACEMENTS OF A THIN BLADE SUBJECTED TO TURBULENT BOUNDARY-LAYER-INDUCED RANDOM PRESSURE FLUCTUATIONS FROM BOTH SIDES WHEN WATER IS FLOWING ALONG THE SHORT SIDE OF THE BLADE FOR U_∞ =16 m s^{-1} AND ζ=10^{-3}.

	Max. total rms displacements (m)			
	Mesh 10×20	Mesh 20×30	Mesh 30×40	Mesh 35×45
U	7.2056E-07	9.0393E-07	1.0855E-06	1.1807E-06
V	4.9851E-07	6.2037E-07	7.4023E-07	8.0318E-07
W	1.7063E-05	2.2161E-05	2.6964E-05	2.9444E-05

The results reveal that the total rms displacements are directly proportional to the free stream velocity and inversely proportional to the damping ratio. The same shift in rms response was observed as the damping ratio changed through all velocities. It is noted that the maximum total rms displacements are small for the set of calculations, as expected.

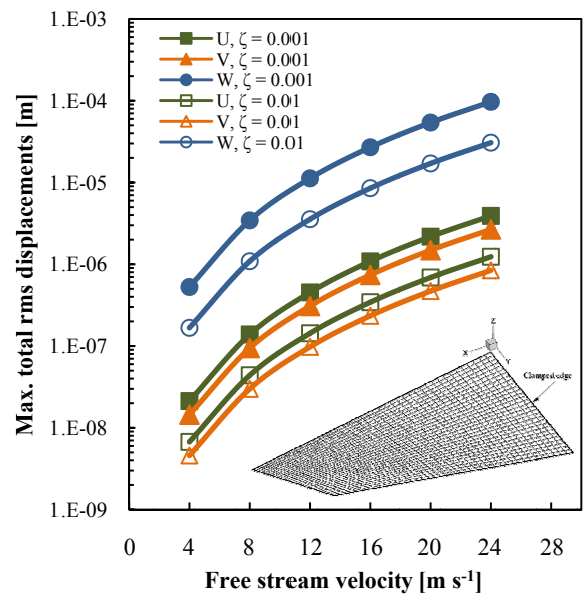

FIGURE 4. MAXIMUM TOTAL RMS DISPLACEMENTS OF A CURVED BLADE SUBJECTED TO A TURBULENT BOUNDARY-LAYER-INDUCED PRESSURE FIELD FROM BOTH SIDES.

9. CONCLUSION

In this paper, we have presented a method to predict the total rms displacement response of an open curved thin shell structure to a random pressure field originating from a turbulent boundary layer in subsonic flow. This research is based on a method previously developed by the authors to predict the dynamic behavior of three-dimensional curved thin shells in the vicinity of fluid. The formulation of the dynamic problem is a combination of classic thin shell theory and finite element analysis in which the finite elements are four-noded flat shell elements with five degrees of freedom per node. This method is capable of calculating both high and low frequencies, which are of great importance for determining the response of structures subjected to turbulent random pressure fields. Dynamic characteristics of the

structure in a vacuum and in contact with fluid such as mode shapes in a vacuum and wetted natural frequencies obtained using a method previously developed by the authors are incorporated into the calculation of random response. A random pressure field is estimated at each node of the finite element. Description of the turbulent pressure field is based on the Corcos formulation for the cross spectral density of pressure fluctuations. Exact integrations over surface and frequency lead to an expression for the rms displacement response in terms of the wetted natural frequency of the system, undamped mode shapes, generalized mass matrix and other characteristics of the structure and flow.

An in-house program was developed to calculate the total root mean square displacement response of a thin structure to random vibration due to a turbulent boundary layer of subsonic flow. To the author's knowledge, there is no reference in the literature for the total rms displacement of an open curved thin shell structure subjected to such random pressure. Therefore, in order to validate our method a cylindrical shell was analyzed and the total rms radial displacement was predicted and compared favorably with that obtained using software developed by Lakis and Païdoussis using cylindrical element and a hybrid finite element method. Curved thin shell structures with discontinuities in thickness and material properties under different boundary conditions subjected to various boundary conditions of fluid can also be investigated. As a future study, this method can be applied to analyze a system of blades subjected to a turbulent boundary layer.

REFERENCES

[1] H. P. Bakewell, G. F. Carey, J. J. Libuka, H. H. Schloemer, and W. A. Von Winkle, "Wall pressure correlations in turbulent pipe flow," U. S. Navy Underwater Sound Laboratory, New London, CT. Report No. 559, 1962.

[2] G. M. Corcos, "Structure of turbulent pressure field in boundary-layer flows," *Journal of Fluid Mechanics*, vol. 18, pp. 353-378, 1964.

[3] W. W. Willmarth and C. E. Wooldridge, "Measurements of fluctuating pressure at wall beneath thick turbulent boundary layer," *Journal of Fluid Mechanics*, vol. 14, pp. 187-210, 1962.

[4] M. K. Bull, "Wall-pressure fluctuations associated with subsonic turbulent boundary layer flow," *Journal of Fluid Mechanics*, vol. 28, pp. 719-764, 1967.

[5] M. G. Cottis and J. G. Jasonides, "Excitation of finite cylindrical shells by boundary-layer pressure fluctuations (A)," *Journal of Acoustical Society of America*, vol. 36, pp. 1046, 1964.

[6] J. M. Clinch, "Prediction and measurement of the vibrations induced in thin-walled pipes by the passage of internal turbulent water flow," *Journal of Sound and Vibration*, vol. 12, pp. 429-451, 1970.

[7] A. A. Lakis and M. P. Païdoussis, "Prediction of the response of a cylindrical shell to arbitrary or boundary-layer-induced random pressure fields," *Journal of Sound and Vibration*, vol. 25, pp. 1-27, 1972.

[8] F. Birgersson, N. S. Ferguson, and S. Finnveden, "Application of the spectral finite element method to turbulent boundary layer induced vibration of plates," *Journal of Sound and Vibration*, vol. 259, pp. 873-891, 2003.

[9] S. Finnveden, F. Birgersson, U. Ross, and T. Kremer, "A model of wall pressure correlation for prediction of turbulence-induced vibration," *Journal of Fluids and Structures*, vol. 20, pp. 1127-1143, 2005.

[10] D. Mazzoni, "An efficient approximation for the vibro-acoustic response of a turbulent boundary layer excited panel," *Journal of Sound and Vibration*, vol. 264, pp. 951-971, 2003.

[11] S. De Rosa and F. Franco, "Exact and numerical responses of a plate under a turbulent boundary layer excitation," *Journal of Fluids and Structures*, vol. 24, pp. 212-230, 2008.

[12] F. Birgersson, S. Finnveden, and G. Robert, "Modelling turbulence-induced vibration of pipes with a spectral finite element method," *Journal of Sound and Vibration*, vol. 278, pp. 749-772, 2004.

[13] E. Ciappi, F. Magionesi, S. De Rosa, and F. Franco, "Hydrodynamic and hydroelastic analyses of a plate excited by the turbulent boundary layer," *Journal of Fluids and Structures*, vol. 25, pp. 321-342, 2009.

[14] M. Esmailzadeh, A. A. Lakis, M. Thomas, and L. Marcouiller, "Prediction of the response of a thin structure subjected to a turbulent boundary-layer-induced random pressure field," *Journal of Sound and Vibration*, vol. 328, pp. 109-128, 2009.

[15] M. Esmailzadeh, A. A. Lakis, M. Thomas, and L. Marcouiller, "Three-dimensional modeling of curved structures containing and/or submerged in fluid," *Finite Elements in Analysis and Design*, vol. 44, pp. 334-345, 2008.

[16] G. M. Corcos, "Resolution of pressure in turbulence," *Journal of the Acoustical Society of America*, vol. 35, pp. 192-199, 1963.

[17] W. K. Blake, *Mechanics of Flow-Induced Sound and Vibration, Vol. II: Complex Flow-Structure Interaction*. London: Academic Press Inc., 1986.

[18] H. P. Bakewell, "Turbulent wall-pressure fluctuations on a body of revolution," *Journal of the acoustical society of America*, vol. 43, pp. 1358-1363, 1968.

[19] M. K. Au-Yang, *Flow-Induced Vibration of Power and Process Plant Components*. New York: ASME Press, 2001.

[20] M. Esmailzadeh, A. A. Lakis, M. Thomas, and L. Marcouiller, "Three-dimensional modeling of curved structures containing and/or submerged in fluid," Department of Mechanical Engineering, École Polytechnic of Montreal Technical report EPM-RT-2006-06, 37 pages, June 2006.

[21] A. A. Lakis and M. P. Païdoussis, "Dynamic analysis of axially non-uniform thin cylindrical shells," *Journal of Mechanical Engineering Science*, vol. 14, pp. 49-71, 1972.

[22] A. A. Lakis, G. Brusuc, and M. Toorani, "Fluid free surface effect on the vibration analysis of cylindrical shells," presented at Societe Francaise d'Energie Nucleaire - International Congress on Advances in Nuclear Power Plants - ICAPP 2007, "The Nuclear Renaissance at Work", Nice, France, 2008.

[23] A. A. Lakis and S. Neagu, "Free surface effects on the dynamics of cylindrical shells partially filled with liquid," *Journal of Sound and Vibration*, vol. 207, pp. 175-205, 1997.

[24] A. A. Lakis and A. Laveau, "Non-linear effects on the dynamic analysis of cylindrical shells containing a flowing fluid," presented at American Society of Mechanical Engineers, Pressure Vessels and Piping Division (Publication) PVP, Nashville, TN, USA, 1990.